JOURNAL OF APPLIED ELECTROCHEMISTRY **26** (1996) 1111–1115

A cyclic voltammetric study on the electrocatalysis of alkaline iron-electrode reactions

M. K. RAVIKUMAR, T. S. BALASUBRAMANIAN, A. K. SHUKLA

Solid State and Structural Chemistry Unit, Indian Institute of Science, Bangalore 560 012, India

S. VENUGOPALAN

ISRO Satellite Centre, Bangalore 560 017, India

Received 30 August 1995; revised 30 January 1996

The electrocatalysis of charge/discharge reactions of alkaline-iron electrodes with and without the Bi_2S_3 additive have been studied using cyclic voltammetry at different sweep rates and temperatures. The activation energy barriers for the iron-dissolution reaction on the iron electrodes with and without the sulfide additive are found to be 11.5 and 35.5 kJ mol^{-1}, respectively, suggesting that the presence of sulfide additive in iron-active material lowers the activation barrier for the iron dissolution reaction appreciably.

1. Introduction

The charge/discharge reactions at the negative electrode of the nickel–iron cell occur in two steps [1, 2]. The first step involves conversion of iron to α-$Fe(OH)_2$ which transforms to δ-FeOOH in the second step during discharge. However, only the first step is considered important for battery applications. The iron active material is retrieved during the charging process. The charge/discharge processes of the alkaline iron electrode may be represented as

$$Fe + 2OH^- \underset{\text{charge}}{\overset{\text{discharge}}{\rightleftharpoons}} Fe(OH)_2 + 2e^- \quad (1)$$

$$Fe(OH)_2 + OH^- \underset{\text{charge}}{\overset{\text{discharge}}{\rightleftharpoons}} FeOOH + H_2O + e^- \quad (2)$$

The standard potentials for Reactions 1 and 2 are −0.87 V and −0.55 V, respectively [3, 4]. The mechanism of the electrode Reaction 1 involves both solid and liquid phases (heterogeneous mechanism) with a dissolution intermediate, $HFeO_2^-$ [5–7]. Thus, the actual course of the electrode Reaction 1 is

$$Fe + 3OH^- \rightleftharpoons HFeO_2^- + H_2O + 2e^- \quad (3)$$

$$HFeO_2^- + H_2O \rightleftharpoons Fe(OH)_2 + OH^- \quad (4)$$

By contrast, Reaction 2 involves diffusion of protons between $Fe(OH)_2$ and δ-FeOOH lattices and the mechanism involved is homogeneous in nature [8, 9].

The open-circuit voltage of a charged iron electrode is always more negative than the hydrogen electrode in the same solution [10, 11]. Consequently, iron is thermodynamically unstable and suffers corrosion through local cells with hydrogen evolution as the conjugate reaction. These reactions are represented as

$$Fe + 2OH^- \longrightarrow Fe(OH)_2 + 2e^- \quad (5)$$

and

$$2H_2O + 2e^- \longrightarrow H_2 + 2OH^- \quad (6)$$

The standard potentials for Reactions 5 and 6 are −0.87 V and −0.82 V, respectively. Owing to the above corrosion reactions, the alkaline iron-electrodes undergo a self-discharge of about 1% to 2% of their nominal capacity per day at 25 °C. Hydrogen evolution also occurs concomitantly while charging the alkaline iron electrodes, resulting in a decrease in their charge acceptance. The degree of utilization (or the faradaic efficiency) of the iron electrode, based on Reaction 1, varies from about 30% for electrodes of commercial iron to 60% for electrodes of high purity iron [12].

The key problems in the development of nickel–iron batteries are the high rate of self-discharge and passivation of the iron electrode. As explained above, the iron electrode undergoes self-discharge as a result of the corrosion reactions. Various additives have been incorporated with the iron active material to suppress corrosion [13–15], and recent studies have demonstrated that a substantial improvement in the overall performance of nickel–iron cells is achievable by doping with certain sulfide additives such as Bi_2S_3 [16–18]. In this communication, we report a study on the electrocatalysis of charge/discharge reactions of alkaline iron electrodes with and without Bi_2S_3 additive employing cyclic voltammetry with different sweep rates at varying temperatures. The study suggests that addition of Bi_2S_3 to the active material lowers the activation barrier for the iron electrode discharge (Reaction 1) to 11.5 kJ mol^{-1} as compared to the activation barrier of 35.5 kJ mol^{-1} for the iron

0021-891X

electrode without sulfide additive. Although there are several studies on the role of sulfide ions in improving the performance of alkaline iron electrode, to our knowledge the present study provides the first quantitative data on the activation barrier for Reaction 1 of the porous alkaline iron electrode. Such data are seminal to the performance of iron electrodes in battery systems.

2. Experimental details

2.1. *Preparation of iron electrodes*

The preparation of the active material and electrode fabrication for the iron electrode is described elsewhere [18]. In brief, the active material was obtained by vacuum decomposition of ferrous oxalate at 500 °C. The active material comprises 15 wt % of Fe and 85 wt % of Fe_3O_4. Iron electrodes without sulfide additive were prepared by ultrasonicating 833 mg of active material, 100 mg of finely divided graphite, 5 mg of $NiSO_4$ in dil. KOH and 62 mg of PTFE as GP-2 Fluon^{TM} suspension. The resulting putty-like mass was rolled against a smooth steel plate. The rolled sheet of the active material was folded around a degreased nickel mesh with a geometrical area of 6.5 cm^2 (2.3 cm × 2.8 cm) and pressed at a pressure of 675 kg cm^{-2} for 5 min. Iron electrodes with sulfide additive were prepared in a similar fashion from 823 mg of active material, 100 mg of finely divided graphite, 5 mg of $NiSO_4$ in dil. KOH, 10 mg of Bi_2S_3 and 62 mg of PTFE as GP-2 Fluon^{TM} suspension. The electrodes were baked at 350 °C for 30 min in a stream of nitrogen gas. The geometrical area of the electrode was 13 cm^2. The current densities are based on the geometrical area of the electrodes.

2.2. *Formation of iron electrodes*

Iron electrodes thus prepared were subjected to formation in electrochemical cells containing 6 M KOH electrolyte with 1 wt % LiOH and sintered nickel oxide electrodes on either side of the iron electrodes to form nickel-iron secondary cells. The cells were provided with an outer jacket for water circulation to maintain the cell temperature to the desired value. The potential of the iron electrode was measured using a Hg/HgO, OH^- (6 M KOH) reference electrode (MMO). During the first formation cycle, the electrodes were charged at $C/20$ rate for 16 h and subsequently at $C/10$ rate for the same period. The discharge rate for the electrode was kept at $C/5$ rate. All the electrodes were found to be formed within 3–5 charge/discharge cycles.

2.3. *Cyclic voltammetric characterization of iron electrodes*

Cyclic voltammograms on fully-charged (SOC ≈ 1) iron electrodes both with and without Bi_2S_3 additive were obtained at various sweep rates in the temperature range 10–40 °C employing a Solatron-1286 electrochemical interface.

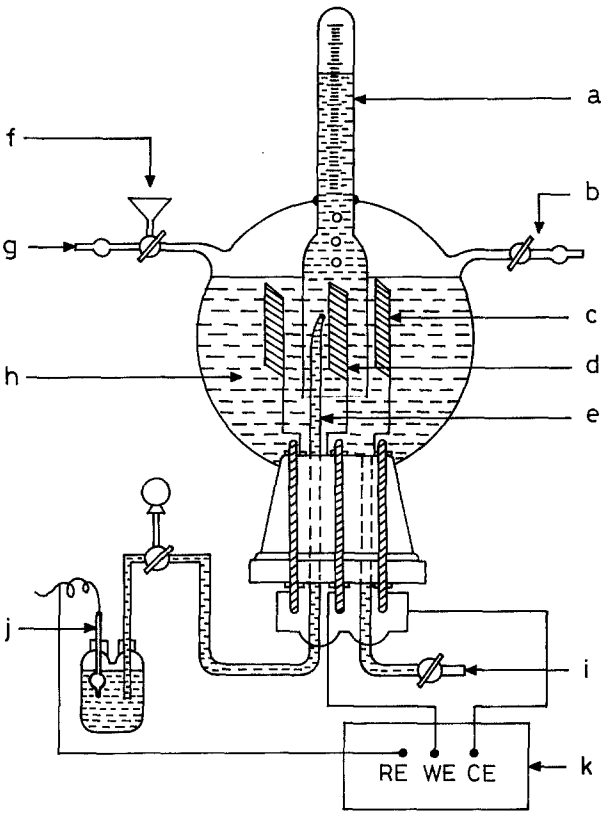

Fig. 1. Experimental setup for gasometric studies: (a) graduated glass tubing, (b) opening to air, (c) counter electrodes, (d) working electrode, (e) luggin capillary, (f) funnel, (g) hydrogen gas inlet, (h) electrolyte, (i) drain tube, (j) reference electrode and (k) potentiostat.

2.4. *Gasometric studies*

Gasometric studies on fully-charged (SOC ≈ 1) iron electrode, both with and without Bi_2S_3 additive, were conducted with the setup shown in Fig. 1. The electrolyte was purged sufficiently with hydrogen gas prior to the experiments. The volumes of hydrogen (V_{H_2}) evolved in cm^3 at the test electrodes at normal temperature and pressure (NTP) during their potentiostatic polarization employing a Wenking potentiostat (model LB 81) were estimated. All V_{H_2} measurements were performed at room temperature (~25 °C) in the cathodic direction over the potential range from −0.93 to −1.05 V vs MMO.

3. Results and discussion

Cyclic voltammograms (scan rate 1 mV s^{-1} and temperature 25 °C) of iron electrodes with and without Bi_2S_3 additive are shown in Fig. 2(a) and (b), respectively. In the cyclic voltammogram of the iron electrode with Bi_2S_3 additive, the three anodic peaks are observed at −0.98 (I), −0.83 (II), and −0.63 V (III) vs MMO and the three cathodic peaks at −0.94 (IV), −1.07 (V) and −1.24 V (VI) vs MMO. The voltammogram of the iron electrode without the additive exhibits three anodic peaks at −0.97 (I), −0.77 (II) and −0.45 V (III) vs MMO and

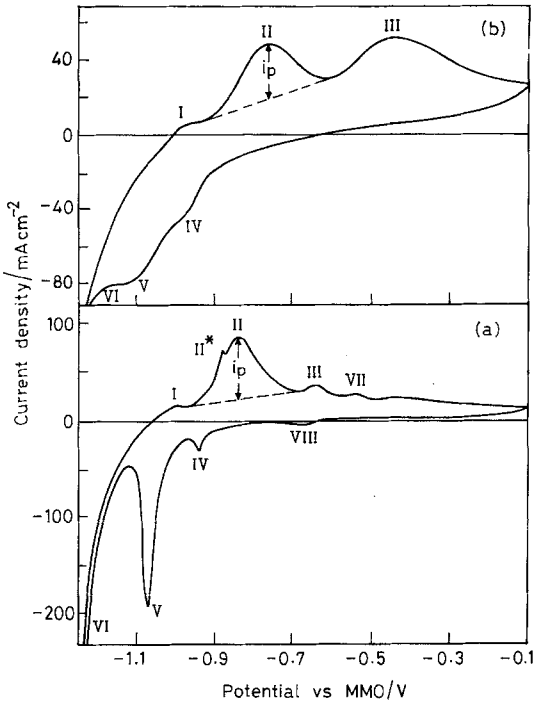

Fig. 2. Cyclic voltammograms of iron electrodes (a) with and (b) without Bi_2S_3 additive at 25 °C (scan rate 1 mV s^{-1}).

corresponding cathodic peaks at −0.98 (IV), −1.16 (V) and −1.25 V (VI) vs MMO (Fig. 2(b)). In these voltammograms, peak I observed in the anodic direction may be attributed to the formation of the initial α-$Fe(OH)_2$ layers or oxidation of adsorbed hydrogen atoms [15, 19–24], while peaks II/V and peaks III/IV are due to the redox couples of the iron electrode reactions, Reactions 1 and 2, respectively [19–24]; peak VI in the cathodic direction represents hydrogen evolution at the iron electrode. The voltammogram of the iron electrode with Bi_2S_3 additive exhibits two additional peaks VII/VIII at −0.52/−0.66 V which are most likely due to the Fe/FeOOH redox couple (Fig. 2(a)). In addition peak II*, observed at −0.89 V vs MMO during the anodic sweep in the voltammogram of the iron electrode with Bi_2S_3 additive, is possibly due to the formation of FeS as reported by Berger and Haschka [25].

A comparison of the potentiodynamic behaviour of the iron electrodes with and without Bi_2S_3 additive suggests:

(i) During the anodic sweeps the peak potentials corresponding to Reactions 1 and 2 for the iron electrode with Bi_2S_3 additive are more cathodic than the iron electrode without the additive.

(ii) The separation in the peak potential for Reaction 1 of the iron electrode with Bi_2S_3 is smaller in

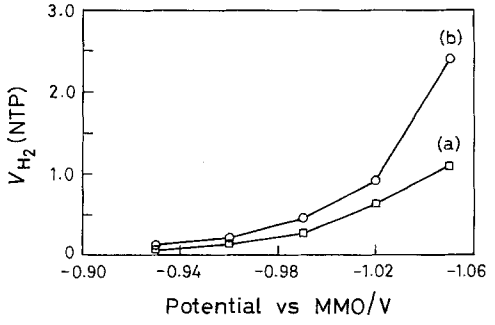

Fig. 3. V_{H_2} (NTP) at various fixed potentials over 2 h duration for iron electrodes (a) with and (b) without Bi_2S_3 additive.

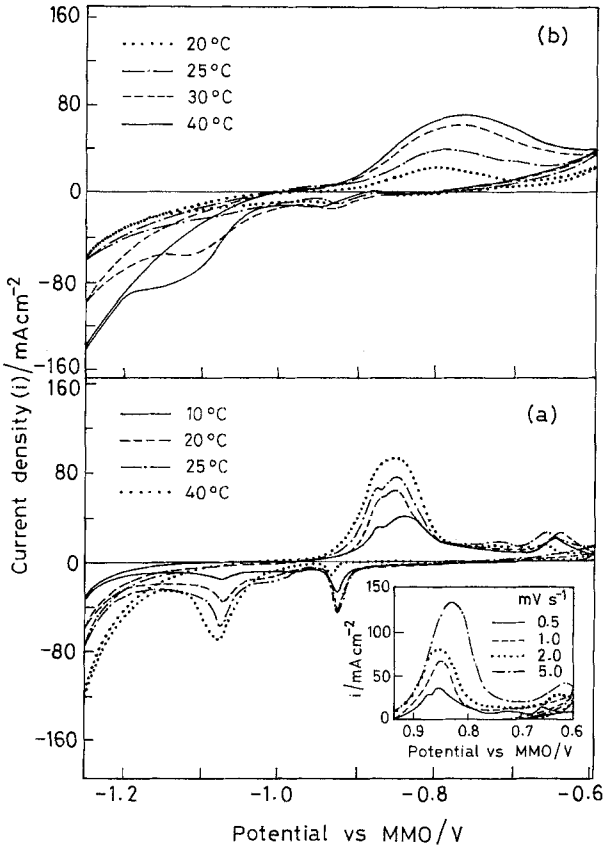

Fig. 4. Effect of varying temperature on the cyclic voltammogram of iron electrodes (a) with and (b) without Bi_2S_3 additive at a scan rate of 0.5 mV s^{-1}; inset shows the effect of varying scan rate at 25 °C.

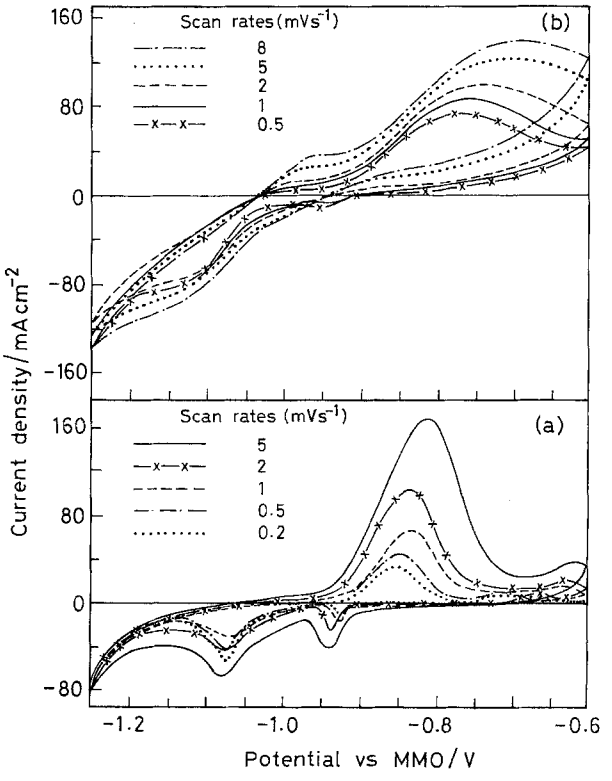

Fig. 5. Effect of varying scan rate on the cyclic voltammogram of the iron electrodes (a) with and (b) without Bi_2S_3 additive at 40 °C.

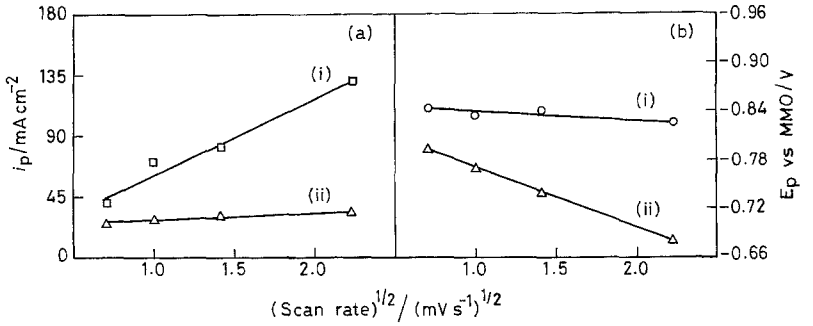

Fig. 6. Variation of (a) peak current density (i_p) and (b) peak potential E_p vs MMO of the peak II with square root of the scan rate on iron electrodes (i) with and (ii) without Bi_2S_3 additive at 25 °C.

relation to the iron electrode without the additive. A similar behaviour is seen for Reaction 2. These features suggest that Reactions 1 and 2 occur more reversibly on the iron electrode with Bi_2S_3 additive.

(iii) Although the peak current density for Reaction 1 on the iron electrode with Bi_2S_3 additive is higher, the peak current density for Reaction 2 is relatively lower than the corresponding value for iron without the additive. This indicates that the passivation of the iron electrode without the additive is larger in relation to that with Bi_2S_3 additive.

(iv) During the cathodic sweep, peaks IV, V and VI are more distinct for the iron electrode with the sulfide additive in relation to the electrode without the additive. Also, the peak current density for Reaction 1, in particular, is much larger for the iron electrode with the sulfide additive.

The volumes of hydrogen (V_{H_2}) evolved at various potentials in the range −0.93 to −1.05 V vs MMO at the alkaline iron electrodes with and without the Bi_2S_3 additive as obtained from the gasometric measurements under potentiostatic charging condition are given in Fig. 3. The data indicate that, although hydrogen evolution occurs on both the electrodes beyond −0.93 V vs MMO, it is more prominent on the electrodes without the sulfide additive. This effect is implicitly seen in the cyclic voltammogram of the electrodes during their cathodic sweep over this potential range.

Figure 4(a) and (b) shows the effect of temperature on the cyclic voltammograms (scan rate 0.5 mV s^{-1}) of the iron electrode with and without Bi_2S_3 additive. It is observed that although the peak potentials for Reaction 1 on the iron electrode with Bi_2S_3 additive remain almost invariant, the corresponding peak current densities increase with temperature. Accordingly, Reaction 1 on the iron electrode with Bi_2S_3 additive is more facile. Interestingly, peak II*, observed during the anodic sweeps in the voltammogram of the iron electrode with Bi_2S_3 additive, disappears (or overlaps) with peak II as the temperature of the electrochemical cell containing the iron electrode is raised from 25 to 40 °C (Fig. 4(a)). A similar effect is observed when the scan rate of the voltammograms at 25 °C is increased from 0.5 mV s^{-1} to a higher value as shown in the inset to Fig. 4(a).

The effect of varying the scan rate of the voltammograms from 0.2 to 5 mV s^{-1} at 40 °C on iron with and without additives is shown in Fig. 5(a) and (b), respectively. It is found that the peak current density for peak II increases monotonically with an anodic shift in the peak potential as the scan rate of the voltammograms is increased from 0.2 to 5 mV s^{-1}.

From the data in Figs 4 and 5, the variation of peak current density and anodic peak-potential for peak II with square root of the scan rate for iron electrodes with and without Bi_2S_3 additive at 25 °C is represented in Fig. 6(a) and (b), respectively. Similar plots are also observed at other temperatures. As seen in Fig. 6, both the peak current density and peak potential for Reaction 1 vary linearly with the square root of scan rate. As the scan rate increases, the peak current density is found to increase with a concomitant decrease in peak potential. Interestingly, the increase in peak current density with the scan rate is higher for the electrode with Bi_2S_3 sulfide additive as opposed to the iron electrode without the additive. In addition, the shift in anodic peak potential is minimal for the iron electrode with Bi_2S_3 additive. This suggests that the formation of passive oxide film is retarded on the iron electrode with Bi_2S_3 additive.

The peak current density, i_p, for peak II can be expressed [26] as

$$i_p = Kv^m \tag{7}$$

where K is the rate constant for the metal dissolution reaction, v is the scan rate, and m is an exponent. Equation 7 can be rewritten as

$$\log i_p = \log K + m \log v \tag{8}$$

The values of the rate constant, K, for the iron electrode reaction (Reaction 1) can be easily estimated from Equation 8. As $v \to 0$, the process is mainly

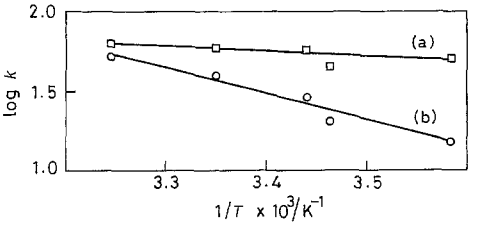

Fig. 7. Arrhenius plots for iron electrodes (a) with and (b) without Bi_2S_3 additive.

activation controlled and i_p represents the corrosion current, i_{cor} [26]. The activation energy, E_a, for iron dissolution (Reaction 1) can then be obtained from the Arrhenius equation [27],

$$E_a = -2.303R\left[\frac{\partial(\log K)}{\partial(1/T)}\right]_V \quad (9)$$

where V is the applied voltage, and R and T have their usual meanings. The respective values of the activation energy, E_a, for the iron-dissolution reaction on the iron electrodes with and without Bi_2S_3 additives, as obtained from the Arrhenius plots given in Fig. 7, are 11.5 and 35.5 kJ mol^{-1}, signifying that the presence of Bi_2S_3 in the iron active material lowers the activation barrier for Reaction 1 quite appreciably.

The iron-electrode discharge reaction (Reaction 1) in alkaline medium proceeds through the following pathways [28–30],

$$Fe + OH^- \longrightarrow Fe(OH)_{ads} + e^- \quad (10)$$

$$Fe(OH)_{ads} + OH^- \longrightarrow [Fe(OH)_2]_{ads} + e^- \quad (11)$$

$$[Fe(OH)_2]_{ads} + OH^- \longrightarrow HFeO_2^- + H_2O \quad (12)$$

$$HFeO_2^- + H_2O \longrightarrow Fe(OH)_2 + OH^- \quad (13)$$

It is noteworthy that the iron-electrode discharge reaction (Reaction 1) is a dissolution-precipitation process with Reaction 11 as the rate determining step. A lower barrier height for Reaction 1 suggests that Reaction 11 proceeds more feasibly in the presence of the sulfide additive.

References

[1] D. Linden, 'Handbook of Batteries', McGraw-Hill, New York (1994).
[2] S. U. Falk and A. J. Salkind, 'Alkaline Storage Batteries', J. Wiley & Sons, New York (1969).
[3] S. Sathyanarayana, The Nickel-Iron Storage Batteries–A Status Report and Techno-economic Survey for India, National Research Development Council of India (1983).
[4] G. Mialzzo and S. Caroli, 'Tables of Standard Electrode Potentials', J. Wiley & Sons, (1978), p. 320.
[5] L. Ojefors, *J. Electrochem. Soc.* **123** (1976) 1139.
[6] R. D. Armstrong and I. Baurhoo, *J. Electroanal. Chem.* **34** (1972) 41.
[7] I. A. Ammar, *Corros. Sci.* **17** (1977) 583.
[8] N. A. Hampson, R. J. Latham, A. Marshall and R. D. Giles, *Electrochim. Acta* **19** (1974) 397.
[9] T. S. Balasubramanium and A. K. Shukla, *J. Appl. Electrochem.* **23** (1993) 947.
[10] L. Ojefors, *Electrochim. Acta* **21** (1976) 263.
[11] P. Hersh, *Trans. Faraday Soc.* **51** (1955) 1442.
[12] A. K. Shukla, M. K. Ravikumar and T. S. Balasubramanian, *J. Power Sources* **51** (1994) 29.
[13] Y. Ramprakash, D. F. A. Koch and R. Woods, *J. Appl. Electrochem.* **21** (1991) 531.
[14] P. R. Vassie and A. C. C. Tseung, *Electrochim. Acta* **21** (1976) 299.
[15] S. Juanto, R. S. Schrebler, J. O. Zabino, J. R. Vilche and A. J. Arvia, *ibid.* **36** (1991) 1143.
[16] K. Vijayamohanan, A. K. Shukla and S. Sathyanarayana, *J. Electroanal. Chem.* **289** (1990) 55.
[17] T. S. Balasubramanian and A. K. Shukla, *J. Power Sources* **41** (1993) 99.
[18] T. S. Balasubramanian, PhD thesis, Indian Institute of Science, Bangalore (1994).
[19] R. S. S. Guzman, J. R. Vilche and A. J. Arvia, *J. Appl. Electrochem.* **11** (1981) 551.
[20] O. A. Albani, J. O. Zerbino, J. R. Vilche and A. J. Arvia, *Electrochim. Acta* **31** (1986) 1403.
[21] J. Černý and K. Micka, *J. Power Sources* **25** (1989) 111.
[22] G. P. Kalaignan, V. S. Muralidharan and K. I. Vasu, *J. Appl. Electrochem.* **17** (1987) 1083.
[23] R. S. S. Guzman, J. R. Vilche and A. J. Arvia, *Electrochim. Acta* **24** (1979) 395.
[24] B. Andersson and L. Ojefors, *J. Electrochem. Soc.* **123** (1976) 824.
[25] G. Berger and F. Haschka, *in* 'Power Sources 11' (edited by L. J. Pearce) Taylor and Francis, Hampshire, UK (1986), p. 237.
[26] A. Wieckowski and E. Ghali, *Electrochim. Acta* **30** (1988) 1423.
[27] M. R. Tarasevich, E. D. German and G. Yu. Borover, *J. Electroanal. Chem.* **204** (1986) 69.
[28] D. W. Shoesmith, P. Taylor, M. G. Bailey and B. Ikeda, *Electrochim. Acta* **23** (1978) 903.
[29] S. Asakura and K. Nobe, *J. Electrochem. Soc.* **118** (1991) 13.
[30] D. M. Dražić and C. S. Hao, *Electrochim. Acta* **27** (1982) 1409.